Raman spectroscopy of orthorhombic perovskitelike $YMnO_3$ and $LaMnO_3$

M. N. Iliev
Texas Center for Superconductivity, University of Houston, Houston, Texas 77204-5932

M. V. Abrashev*
Institut für Festkörperphysik, Technische Universität Berlin, D-10623 Berlin, Germany

H.-G. Lee
Texas Center for Superconductivity, University of Houston, Houston, Texas 77204-5932

V. N. Popov
Faculty of Physics, University of Sofia, 1126 Sofia, Bulgaria

Y. Y. Sun
Texas Center for Superconductivity, University of Houston, Houston, Texas 77204-5932

C. Thomsen
Institut für Festkörperphysik, Technische Universität Berlin, D-10623 Berlin, Germany

R. L. Meng and C. W. Chu
Texas Center for Superconductivity, University of Houston, Houston, Texas 77204-5932
(Received 25 June 1997)

The Raman-active phonons in orthorhombic perovskitelike $YMnO_3$ and $LaMnO_3$ were studied by measuring Raman spectra in various scattering configurations. The experimental Raman line wave numbers and the expected shapes for the phonon modes were compared to those reported for other perovskitelike compounds with the $Pnma$ structure and to the results of lattice dynamical calculations. The observed Raman lines in the spectra of $YMnO_3$ and $LaMnO_3$ were assigned to definite atomic motions. The much larger linewidths and strong variation of the Raman spectra with increasing laser power in the case of $LaMnO_3$ provide evidence for a structural instability that may result in a phase transition under laser annealing. [S0163-1829(98)02506-5]

I. INTRODUCTION

At atmospheric pressure $YMnO_3$ crystallizes in a hexagonal structure [space group $P6_3cm$ (C_{6v}^3), $Z=6$], similar to the rare-earth manganites $RMnO_3$, for R with smaller ionic radius (R=Ho, Er, Tm, Yb, Lu).[1] Upon annealing under high pressures,[2] however, $YMnO_3$ can be converted to its orthorohombic phase [space group $Pnma(D_{2h}^{16})$, $Z=4$, see Fig. 1]. The latter structure is typical for $RMnO_3$ compounds with R of larger ionic radius (R=La, Ce, Pr, Nd, Sm, Eu, Gd, Tb, or Dy).[3,4]

The properties of $RMnO_3$ have been studied intensively since it was found that partial substitution of R by Ca, Sr, or Ba results in structural changes and the occurrence of colossal magnetoresistance near the temperatures of spin ordering of Mn ions.[5] Although it is plausible to expect that structural changes and magnetic ordering will also influence the phonon spectra, these are not well known. While Raman spectra of other orthorhombically distorted perovskites with $Pnma$ structure, in particular rare-earth and yttrium aluminates,[6] orthochromates,[6] and orthoferrites,[7,8] have been reported, there are practically no data on the Raman scattering from orthomanganites. Similarly, only limited information on the infrared phonons of orthomanganites is available in an earlier work of Subba Rao *et al.*[9] on the infrared transmission of RZO_3 (R=rare earth or Y; Z=Cr, Mn, or Fe).

In this paper, using the examples of $YMnO_3$ and $LaMnO_3$, we analyze the Raman spectra and Raman active phonon modes in yttrium and rare earth orthomanganates. The experimentally determined wave numbers and symme-

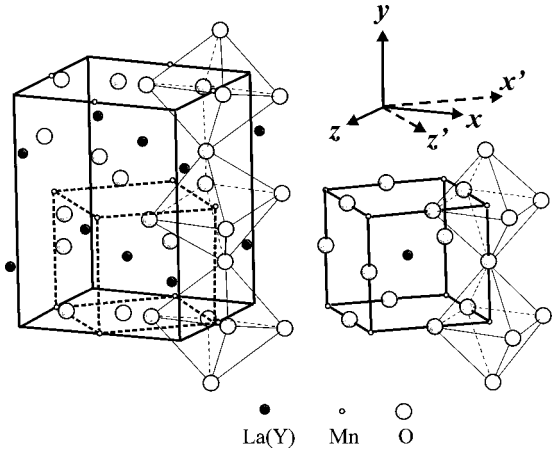

FIG. 1. Unit cell of orthorhombic $RMnO_3$ (R=Y,La; space group $Pnma$). The unit cell of the simple perovskite structure is also shown (right). Empty circles stay for oxygen atoms outside the unit cell.

TABLE I. Wyckoff notations, atomic site symmetries, fractional atomic coordinates, and the irreducible representations for the atoms in orthorhombic $YMnO_3$ and $LaMnO_3$ (in brackets).

Atom	Wyckoff notation	Site symmetry	x	y	z	Irreducible representantions
Y (La)	4(c)	C_s	0.0805 (0.0513)	0.2500 (0.2500)	0.9824 (0.9814)	$2A_g+B_{1g}+2B_{2g}+B_{3g}+$ $+A_u+2B_{1u}+B_{2u}+2B_{3u}$
Mn	4(b)	C_i	0.0000 (0.0000)	0.0000 (0.0000)	0.5000 (0.5000)	$3A_u+3B_{1u}+3B_{2u}+3B_{3u}$
O1	4(c)	C_s	0.4964 (0.4849)	0.2500 (0.2500)	0.1521 (0.0778)	$2A_g+B_{1g}+2B_{2g}+B_{3g}+$ $+A_u+2B_{1u}+B_{2u}+2B_{3u}$
O2	8(d)	C_1	0.3063 (0.3085)	0.0595 (0.0408)	0.7071 (0.7227)	$3A_g+3B_{1g}+3B_{2g}+3B_{3g}$ $+3A_u+3B_{1u}+3B_{2u}+3B_{3u}$

Modes classification

$\Gamma_{\text{Raman}}=7A_g+5B_{1g}+7B_{2g}+5B_{3g}$
$A_g\rightarrow\alpha_{xx},\alpha_{yy},\alpha_{zz}$
$B_{1g}\rightarrow\alpha_{xy},\alpha_{yx}$
$B_{2g}\rightarrow\alpha_{xz},\alpha_{zx}$
$B_{3g}\rightarrow\alpha_{yz},\alpha_{zy}$

$\Gamma_{\text{ir}}=9B_{1u}+7B_{2u}+9B_{3u}$
$\Gamma_{\text{silent}}=8A_u$
$\Gamma_{\text{acoustic}}=B_{1u}+B_{2u}+B_{3u}$

tries of Raman lines are compared to results of lattice dynamical calculations (LDC's). This allowed us to assign most of the observed Raman lines to phonon modes involving definite atomic motions. It was also found that the lines in the Raman spectra of $LaMnO_3$ are much broader and, as a whole, the spectra change significantly upon variations in the incident laser power. Such a behavior indicates a structural instability and a possibility for a laser-annealing-induced structural phase transition.

II. MATERIALS AND METHODS

A. Sample preparation and characterization

$YMnO_3$. As a first step in sample preparation, ceramic pellets of hexagonal $YMnO_3$ (space group $P6_3cm$) were synthesized following a procedure described elsewhere.[10] In a second step, the hexagonal samples were resintered in a high pressure furnace under 30 kbar at 1010 °C for 3 h (or at 960 °C for 4 h). The room-temperature x-ray-diffraction (XRD) pattern were collected using a Rigaku DMaxIII/B x-ray diffractometer. The XRD pattern corresponded to a single-phase orthorhombic structure with lattice parameters $a=5.8444(9)$ Å, $b=7.3579(3)$ Å, and $c=5.2616(0)$ Å: values very close to those reported in Ref. 2 for orthorhombic $YMnO_3$. To obtain the atomic site positions in $YMnO_3$, a structural refinement was carried out with the RIETA-94 refinement program. The fractional atomic coordinates are given in Table I.

$LaMnO_3$. The $LaMnO_3$ samples were prepared following a procedure similar to the one described in Refs. 11 and 12. First, the rhombohedral phase $LaMnO_3$ (space group $R\bar{3}c$) was prepared by solid state reaction and calcinated in air at 900 °C. Then the material was twice reground, pressed, and sintered in air at 1100 and 1200 °C for 15–30 h. The orthorhombic phase was prepared by heating the rhombohedral phase under N_2 flow at 900 °C. The lattice parameters corresponded to these of Ref. 4. It was therefore reasonable to use in our lattice dynamical calculation the fractional atomic coordinates and interatomic distances cited in that paper. These atomic coordinates are also given in Table I.

B. Raman measurements

The Raman spectra were obtained at room temperature with two different experimental setups: (i) a Mole S3000 triple spectrometer with Si-diode array detector and (ii) a Labram single spectrometer with a charge coupled device detector and appropriate notch filters. In each setup an objective of $\times 100$ magnification was used both to focus the laser beam on the sample surface and to collect the scattered light. The 514.5 nm Ar^+ laser or 632.8 nm He-Ne lines were used for excitation. As a rule, the laser power at the focus spot (2–3 μm in diameter) was kept below 2 mW for $YMnO_3$ and 0.2 mW for $LaMnO_3$ to avoid structural transformations due to overheating. Laser annealing experiments with higher focused laser power (up to 5 mW) were also performed for $LaMnO_3$.

To obtain Raman spectra with a known scattering configuration the reasonable assumption was made that similarly to simple ABO_3 perovskites where the as-grown crystal edges (and surfaces) are parallel to the B-O bonds and the straight edges exhibited by many $YMnO_3$ and $LaMnO_3$ microcrystals are parallel to the strong Mn-O bonds. More precisely, for the *Pnma* structure straight edges are expected along the x', y, and z' directions, where y coincides with b, and x' and z' are two mutually orthogonal direction in the ac planes, rotated by 45° with respect to the crystallographic a and c axes, respectively.[13] This assumption was confirmed by the polarization dependencies of experimental Raman spectra.

C. Calculations of the lattice dynamics

The wave numbers of Γ-point phonon modes as well as the amplitudes and directions of corresponding atomic motions were calculated using the shell model with parameters obtained as described earlier in Refs. 10,14. With these parameters, satisfactory results for the lattice dynamics are expected only in the case of weakly distorted perovskites. As follows from Table I, the deviations from the ideal perovskite structure are larger for $YMnO_3$ and smaller for $LaMnO_3$. It is therefore plausible to expect that the shell model we used would better describe the phonons in $LaMnO_3$.

III. CRYSTAL STRUCTURE AND Γ-POINT PHONONS IN ORTHORHOMBIC $YMnO_3$ AND $LaMnO_3$

The unit cell of $LaMnO_3$ with $Pnma$ structure is shown in Fig. 1 (left). This structure contains a network of corner-sharing MnO_6 octahedra and belongs to the family of rotationally distorted perovskites with Glazer's notation $(a^-b^+a^-)$.[15] It can be obtained from the simple perovskite structure [whose unit cell is shown in Fig. 1 (right)] by two consequent rotations of MnO_6 octahedra, namely, (i) Around the [010] direction of cubic perovskite (y axis in $Pnma$); (ii) around the [101] direction of cubic perovskite (x axis in $Pnma$).

Considering qualitatively the structural variations and corresponding changes of the Raman spectra in the orthorhombic $RMnO_3$ series (R=rare earth or Y) compounds, one can assume in a rough approximation that these changes are mainly due to variations in angles of the above-mentioned rotations and to a lesser extent to changes in Mn-O distances. Within such an assumption the MnO_6 octahedra are considered as rigid units. With only the first rotation (i) the structure would be of tetragonal $P4/mbm$ symmetry. With only the second rotation (ii) the structure would be of $Imma$ symmetry.

In Table I are summarized the results of group-theoretical analysis for the Γ-point phonons of orthorhombic $RMnO_3$ (space group $Pnma$, R=Y,La). Of the total 60 Γ-point phonon modes, 24 $(7A_g+5B_{1g}+7B_{2g}+5B_{3g})$ are Raman-active, 25 $(9B_{1u}+7B_{2u}+9B_{3u})$ are infrared-active, $8(8A_u)$ are silent, and $3(B_{1u}+B_{2u}+B_{3u})$ are acoustic modes. Provided the microcrystal edges are along the x', y, or z' directions, the measurements can be done in the following exact scattering configurations: $x'x'(z'z')$, $x'z'(z'x')$, yy, $xx(zz)$, $yx(xy)$, $yx'(x'y)$, and $yz'(z'y)$. Note, that the x' and z' directions are equivalent. Moreover, due to microtwinning, the x and z directions are also indistinguishable. Therefore, the independent exact scattering configurations that can be obtained with the polarizations of the incident and scattered light parallel, perpendicular or at 45° with respect to the straight crystal edges, and the allowed phonon mode symmetries in these configurations are

$$x'x'(z'z') \rightarrow A_g + B_{2g},$$

$$x'z'(z'x') \rightarrow A_g(\text{weak}),$$

$$yy, xx(zz) \rightarrow A_g,$$

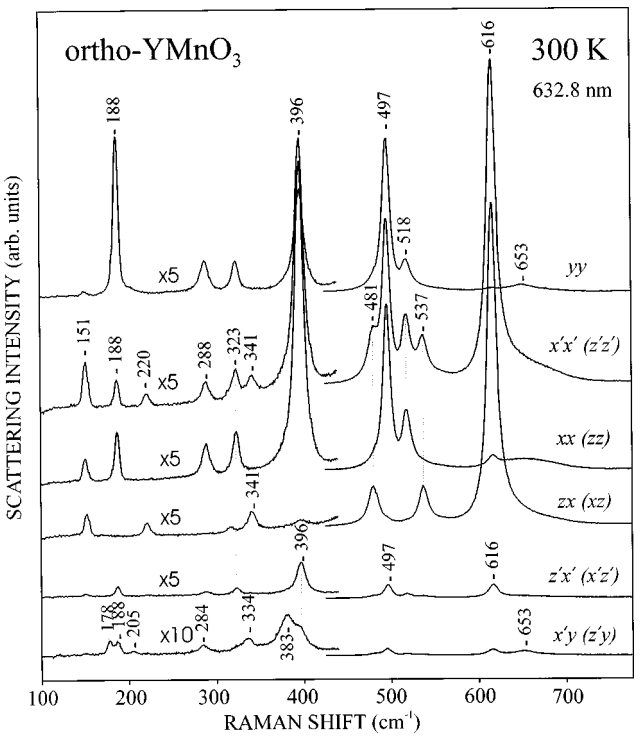

FIG. 2. Raman spectra of orthorhombic $YMnO_3$ in various scattering configurations. The left half of the spectra are multiplied by the factor indicated there.

$$yx'(x'y) \rightarrow B_{1g} + B_{3g},$$

$$xz(zx) \rightarrow B_{2g}.$$

The parallel $x'x'(z'z')$ and yy configurations can be distinguished by the occurrence of additional Raman lines of B_{2g} symmetry in the $x'x'(z'z')$ spectra.

IV. RESULTS AND DISCUSSION

In Fig. 2 the polarized Raman spectra of $YMnO_3$ in the yy, $x'x'(z'z')$, $xx(zz)$, $zx(xz)$, $z'x'(x'z')$, and $x'y(z'y)$ scattering configurations are shown. The lines at 151, 188, 288, 323, 396, 497, and 518 cm^{-1} which are stronger in the *parallel* $[yy, x'x'(z'z'), xx(zz)]$ than in the *crossed* $[z'x'(x'z'), zx(xz), x'y(z'y)]$ polarizations, are obviously of A_g symmetry. The weak line at 653 cm^{-1} in the yy spectrum varies with the sample and seems to be of defect origin. A similar line has been observed at 645 cm^{-1} in $ErFeO_3$ and has been assigned as an impurity-related phonon line[7]. The lines at 220, 317, 341, 481, 537, and 616 cm^{-1} are pronounced in both the $x'x'(z'z')$ and $zx(xz)$ spectra and therefore are of B_{2g} symmetry. Interestingly, a line at 152 cm^{-1} is seen in the $zx(xz)$ spectra, too. This is an indication for a superposition of lines of A_g and B_{2g} symmetry at 151–152 cm^{-1}. As expected, the A_g modes give rise to weak lines also in the $z'x'(x'z')$ spectra, due partly to analyzer leakage, but also to the inequality of the α_{xx} and α_{zz} components of the A_g Raman tensor. In addition to the leakage of the A_g lines one observes in the $x'y(z'y)$ spectra lines at 178, 205, 284, 334, 383, and 653 cm^{-1} (also very weak). These lines have to be of either B_{1g} or B_{3g} symmetry. The

TABLE II. Experimental values of the Raman frequencies for various RZO_3 compounds with $Pnma$ structure. The results of the LDC's for $YMnO_3$ and $LaMnO_3$ are also given. The assignment either indicates the vibrating atoms and the vibrational direction (in brackets) or correspond to mode assignment of Fig. 5. The experimental lines in the $yx'(yz')$ spectra are assigned to modes of B_{1g} or B_{3g} symmetry by comparison to the LDC results.

Mode	$YMnO_3$ exp.	$YMnO_3$ LDC	$LaMnO_3$ exp.	$LaMnO_3$ LDC	Assign ment	$YAlO_3$ (Ref. 6)	$YCrO_3$ (Ref. 6)	$GdCrO_3$ (Ref. 6)	$ErFeO_3$ (Ref. 7)	$HoFeO_3$ (Ref. 8)
A_g	**151**	**104**	**140**	**81**	$R(x)$	150	156	141	112	109
A_g	**188**	**147**	**198**	**162**	$R(z)$	197	188	158	140	139
A_g	**288**	**223**	**257**	**246**	$A_g(2)$	278	282	260	273	270
A_g	**323**	**304**		**263**	O1(x)	345	346	326	345	340
A_g	**396**	**407**	**284**	**326**	$A_g(4)$	412	429	390	434	425
A_g	**497**	**466**	**493**	**480**	$A_g(3)$		492	480	505	495
A_g	**518**	**524**		**582**	$A_g(1)$	553	566	562		
B_{1g}	**205**	**181**	**184**	**182**	$R(y)$					
B_{1g}	**284**	**288**		**254**	$B_{1g}(3)$	270	272	246	264	
B_{1g}	**383**	**342**		**347**	$B_{1g}(4)$	403	413		365	
B_{1g}		**413**		**575**	$B_{1g}(2)$	555				
B_{1g}		**593**		**693**	$B_{1g}(1)$					
B_{2g}	**151**	**137**	**109**	**123**	$R(z)$	157			112	
B_{2g}	**220**	**162**	**170**	**150**	$R(x)$	219	223	161	163	159
B_{2g}	**317**	**285**		**218**	$B_{2g}(4)$					
B_{2g}	**341**	**393**	**308**	**369**	O1(z)	283	318	285	322	
B_{2g}	**481**	**470**	**481**	**464**	$B_{2g}(3)$		502	480	505	
B_{2g}	**537**	**583**		**509**	$B_{2g}(2)$	552				
B_{2g}	**616**	**617**	**611**	**669**	$B_{2g}(1)$					
B_{3g}	**178**	**145**		**158**	$R(y)$	197	176	157		
B_{3g}	**336**	**363**	**320**	**343**	$B_{3g}(4)$					
B_{3g}		**390**		**462**	$B_{3g}(3)$	470	487	472	481	
B_{3g}		**476**		**603**	$B_{3g}(2)$	540	569	568		
B_{3g}		**610**		**692**	$B_{3g}(1)$					

experimental data for orthorhombic $YMnO_3$ are summarized in Table II.

Unlike the case of $YMnO_3$, the Raman spectra of $LaMnO_3$ exhibit an unusually strong dependence on the exciting laser power even at low laser power densities. Indeed, with laser power of 2 mW (used to obtain the spectra of $YMnO_3$ of Fig. 2) the Raman spectra of $LaMnO_3$ consist of broad relatively weak lines superimposed on a stronger structureless background. Figure 3 illustrates the variations of Raman spectra of $LaMnO_3$ with incident laser power between 0.12 and 4.55 mW (the averaged laser power density varies between $\sim 2\times 10^7$ W/m^2 and $\sim 1\times 10^9$ W/m^2). At low laser power density the background is strongly reduced and the Raman lines are relatively narrow, but still much broader than the corresponding lines in the spectra of $YMnO_3$ (see also Fig. 4). Except for a broadening, the increase of laser power results in a considerable shift of some of the spectral features. In particular, the structure with a maximum near 275 cm^{-1} shifts towards lower wave numbers and transforms into a broad peak centered near 220 cm^{-1}.

To explain qualitatively the observed dependence on the laser irradiation let us remember that the structure of $LaMnO_3$ depends on the method of preparation and is sensitive to the actual oxygen content, to the oxygen partial pressure, and to the temperature. Laser annealing increases the temperature thus resulting in increasing disorder and stimulating (at higher temperatures) in- and out-diffusion of oxygen. During irradiation of oxygen-deficient samples in air the in-diffusion of oxygen will prevail. As a result, a structural transformation toward the rhombohedral phase may be expected at higher power densities in the irradiated spot. Indeed, the Raman spectrum of rhombohedral $LaMnO_3$ shown in the bottom of Fig. 3 is very similar to the spectra obtained after irradiation of orthorhombic $LaMnO_3$ with a higher laser power. As expected, at lower power densities (in our case at a laser power below 1.87 mW) the spectral changes are reversible.

Figure 4 shows the Raman spectra of $LaMnO_3$ as obtained with the lowest power density used (2×10^7 W/cm^2) from oriented grains in the same scattering configurations as in the case of $YMnO_3$ (Fig. 2). For comparison the $x'x'(z'z')$ spectrum of $YMnO_3$ as measured with 4×10^8 W/cm^2 is also included. Obviously, the number of pronounced Raman lines in the spectra of $LaMnO_3$ is less than in $YMnO_3$, while their linewidths are larger in spite of much lower laser power used. Lines of A_g symmetry are observed at 140, 198, 257, 284, and 493 cm^{-1}, of B_{2g} symmetry at

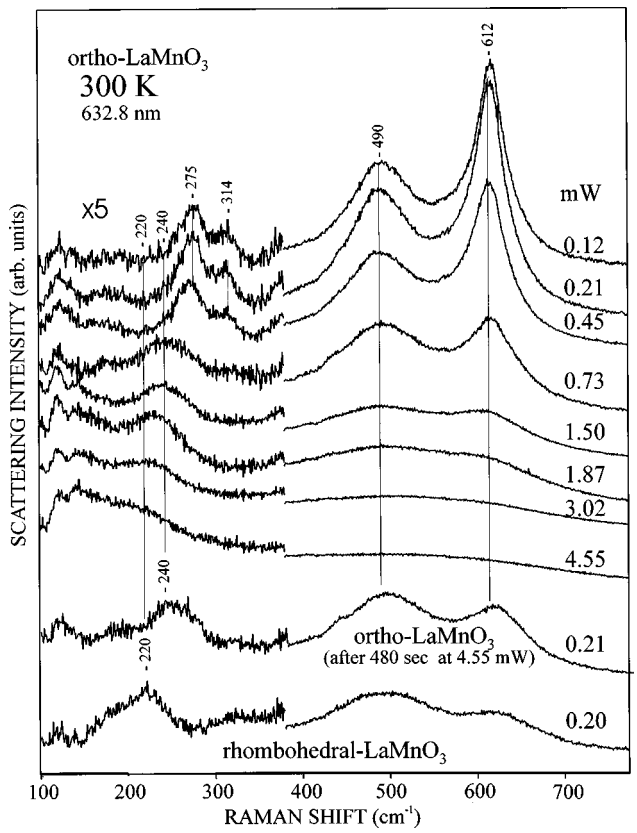

FIG. 3. Raman spectra of orthorhombic $LaMnO_3$ ($Pnma$) as measured with increasing incident laser power. The Raman intensities are normalized to the laser power. The Raman spectrum of rhombohedral $LaMnO_3$ (space group $R\bar{3}c$) is also shown. The left half of the spectra are multiplied by the factor indicated there.

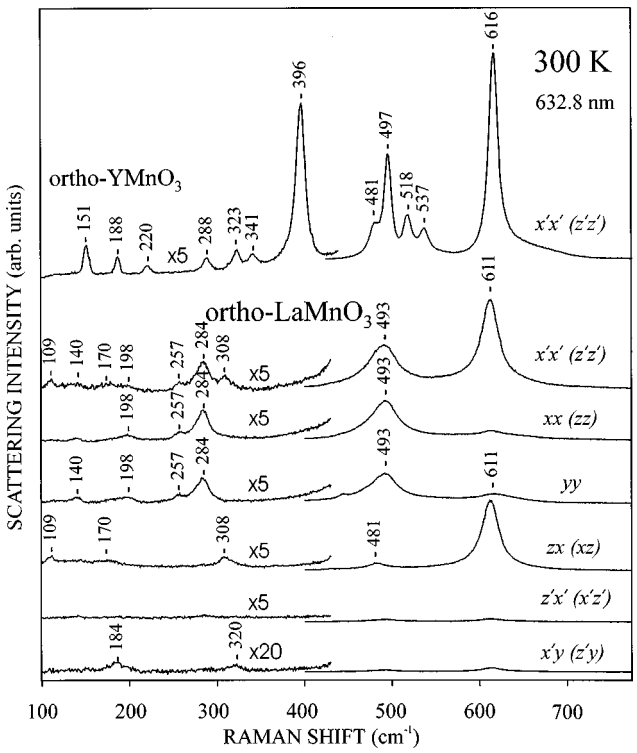

FIG. 4. Raman spectra of orthorhombic $LaMnO_3$ (space group $Pnma$) in various scattering configurations. At the top the zz spectrum of $YMnO_3$ is also given for comparison. The left half of the spectra are multiplied by the factor indicated there.

109, 170, 308, 481, and 611 cm^{-1}, and of B_{1g} or B_{3g} symmetry at 184 and 320 cm^{-1}. The experimentally determined Raman phonon wave numbers for $LaMnO_3$ are also included in Table II.

Further, the assignment of Raman lines of $YMnO_3$ and $LaMnO_3$ to particular atomic motions will be discussed on the basis of Raman line symmetries, some general considerations concerning the expected shapes for the Raman modes, and by comparison to Raman spectra of other RZO_3 compounds with $Pnma$ structure, such as $YAlO_3$,[6] $RFeO_3$ (R=Tb,Dy,Ho,Tm),[8] $ErFeO_3$,[7] $YCrO_3$,[6] and $GdCrO_3$.[6] A comparison to the LDC results for $YMnO_3$ and $LaMnO_3$ will also be made.

The corner-shared ZO_6 octahedra are building units of the RZO_3 compounds with $Pnma$ structure as the Z-O1 and Z-O2 bonds are shorter than the R-O1 and R-O2 ones. The Z atoms (Mn, Al, Fe, or Cr) are in centers of symmetry and do not participate in Raman active modes. Therefore, it is plausible to expect that at least part of the Raman modes will include oxygen motions similar to the characteristic ones for an isolated ZO_6 unit.

Considering the atomic motions constituting the phonon modes of $Pnma$ structure, the following has to be taken into account.

(i) The motions of R and O1 atoms are restricted by the site symmetry (C_s^{xz}) within the xz plane for the A_g and B_{2g} modes, and along the y axis for the B_{1g} and B_{3g} modes. As

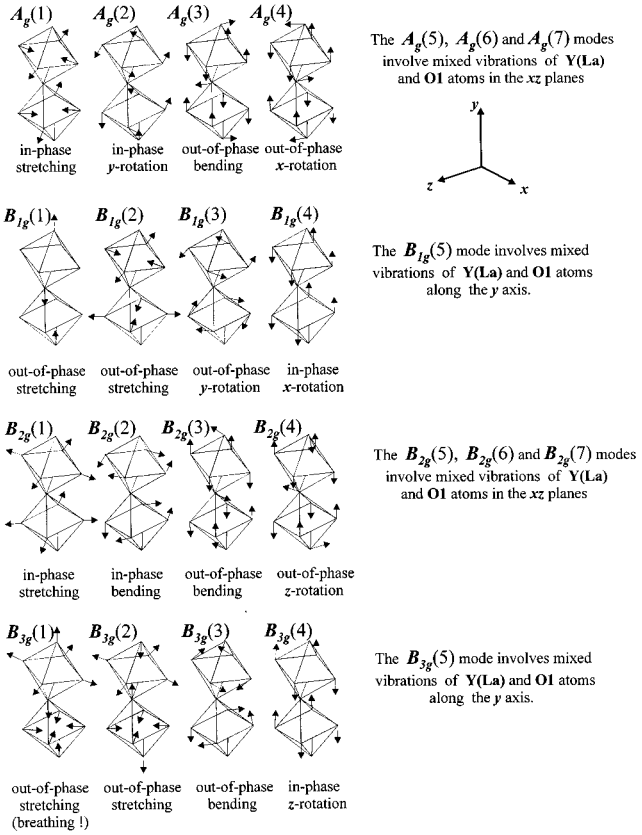

FIG. 5. Raman allowed phonon modes for the RZO_3 compounds with $Pnma$ structure.

for the O2 atoms, their site symmetry (C_1) is low and there are no symmetry restrictions on the direction of O2 vibrations for all Raman modes. Nevertheless, most reasonably, the O2 atoms vibrate nearly along (stretching) or perpendicular (bending or rotation) to the strong Z-O2 bonds.

(ii) The unit cell of RZO_3 compounds contains two ZO_6 octahedra along the y direction and corresponding oxygen atoms in these neighboring octahedra may vibrate in-phase or out-of-phase.

Figure 5 shows schematically the shapes of the four Raman modes of each symmetry (A_g, B_{1g}, B_{2g}, and B_{3g}) involving pure or mixed O1 and O2 vibrations. The remaining Raman modes correspond to mixed R-O1 vibrations either within the xz planes (A_g and B_{2g} modes), or along the y axis (B_{1g} or B_{3g} modes). It follows from our LDC results, however, that at least in the case of $LaMnO_3$ many of nominally ''mixed'' modes are dominated by vibrations of mainly one type of atom and in a good approximation they can be considered as ''pure'' modes.

As follows from Table II, the wave numbers of Raman lines corresponding to the same phonon modes in $YMnO_3$, $YCrO_3$, and $YAlO_3$ are very close. The same is true for $LaMnO_3$ and $GdCrO_3$. Therefore, one can conclude that the atomic vibrations are not sensitive to transition metal ionic radii, which have the values of 0.535, 0.55, 0.58, or 0.615 Å for trivalent sixfold coordinated Al, Fe, Mn, or Cr, respectively.[16] Modes involving motions of mainly R atoms have frequencies following roughly the $m_R^{-1/2}$ dependence.

The LDC and experimental Raman frequencies are in relatively good agreement for $LaMnO_3$. The agreement is not as good, however, for $YMnO_3$, in particular concerning the low frequency Y modes. The discrepancies most likely arise from some approximation in the shell model. In particular, it was assumed that the deviations from the simple perovskite structure are not strong and the averaged R-O distance can be used instead of real R-O distances to define some shell model parameters. While such an assumption is reasonable for $LaMnO_3$, it may not be good for $YMnO_3$ where the distortions of perovskitelike structure are stronger and Y-O bond lengths exhibit significant differences. The changes of R-O distances upon La for Y substitution can alter also the relative weight of forces which determine the R-O interactions.

V. CONCLUSIONS

In conclusion, the Raman spectra of $YMnO_3$ and $LaMnO_3$ were measured and analyzed. The Raman lines were assigned to definite atomic vibrations. The strong variations of the spectral line shape on the excitation laser power in the case of $LaMnO_3$ provide evidence for a structural instability that may result in a laser-irradiation-induced structural phase transition.

ACKNOWLEDGMENTS

One of us (M.V.A.) acknowledges financial support from the Alexander von Humboldt Foundation (Bonn, Germany). This work was supported in part by NSF Grant No. DMR 95-10625, the T. L. L. Temple Foundation, the John J. and Rebecca Moores Endowment, and by the State of Texas through the Texas Center for Superconductivity at the University of Houston.

*Permanent address: Faculty of Physics, University of Sofia, BG-1126 Sofia, Bulgaria.

[1] H. L. Yakel, W. C. Koehler, E. F. Bertaut, and E. F. Forrat, Acta Crystallogr. **16**, 957 (1963).

[2] A. Waintal and J. Chenavas, C. R. Seances Acad. Sci., Ser. B **264**, 168 (1967).

[3] M. A. Gilleo, Acta Crystallogr. **10**, 161 (1957).

[4] F. Moussa, M. Hennion, J. Rodriguez-Carvajal, H. Moudden, L. Pinsard, and A. Revcolevschi, Phys. Rev. B **54**, 15 149 (1996).

[5] See, e.g., D. I. Khomskii and G. A. Sawatzky, Solid State Commun. **102**, 87 (1997).

[6] M. Udagawa, K. Kohn, N. Koshizuka, and T. Tsushima, Solid State Commun. **16**, 779 (1975).

[7] N. Koshizuka and S. Ushioda, Phys. Rev. B **22**, 5394 (1980).

[8] S. Venugopalan, M. Dutta, A. K. Ramdas, and J. P. Remeika, Phys. Rev. B **31**, 1490 (1985).

[9] G. V. Subba Rao, C. N. R. Rao, and J. R. Ferraro, Appl. Spectrosc. **24**, 436 (1970).

[10] M. N. Iliev, H. G. Lee, V. N. Popov, M. V. Abrashev, A. Hamed, R. L. Meng, and C. W. Chu, Phys. Rev. B **56**, 2488 (1997).

[11] I. G. Krogh Andersen, E. Krogh Andersen, P. Norby, and E. Skou, J. Solid State Chem. **113**, 320 (1994).

[12] P. Norby, I. G. Krogh Andersen, E. Krogh Andersen, and N. H. Andersen, J. Solid State Chem. **119**, 191 (1995).

[13] We have in mind the ''averaged'' direction of Mn-O bonds. Due to tilting of MnO_6 octahedra with respect to a, b, and c, the actual Mn-O1 and Mn-O2 bonds are only approximately parallel to the y and $x'(z')$ directions, respectively.

[14] V. N. Popov, J. Phys.: Condens. Matter **7**, 1625 (1995).

[15] A. M. Glazer, Acta Crystallogr., Sect. B: Struct. Crystallogr. Cryst. Chem. **B28**, 3384 (1972).

[16] R. D. Shannon, Acta Crystallogr., Sect. A: Cryst. Phys., Diffr., Theor. Gen. Crystallogr. **A32**, 751 (1976).